Alpha-synuclein accumulates in huntingtin inclusions but forms independent filaments and its deficiency attenuates early phenotype in a mouse model of Huntington´s disease

Cristina Tomás-Zapico[1,2#], María Díez-Zaera[3], Isidre Ferrer[2,4], Pilar Gómez-Ramos[5], María A. Morán[5], M. Teresa Miras-Portugal[3], Miguel Díaz-Hernández[3] and José J. Lucas[1,2]*

[1] Center for Molecular Biology "Severo Ochoa" (CBMSO), CSIC/UAM, Madrid, Spain.

[2] Networking Research Center on Neurodegenerative Diseases (CIBERNED). Instituto de Salud Carlos III, Spain.

[3] Department of Biochemistry and Molecular Biology IV. Facultad de Veterinaria, Universidad Complutense de Madrid, Madrid, Spain.

[4] Institute of Neuropathology, IDIBELL- University Hospital Bellvitge, Barcelona, Spain

[5] Department of Morphology, Facultad de Medicina, Universidad Autónoma de Madrid, Spain

Present address: Department of Functional Biology, Oviedo University, Oviedo, Spain

*Corresponding author: José J. Lucas
Center for Molecular Biology "Severo Ochoa" (CBMSO)
CSIC/UAM
Campus UAM de Cantoblanco
28049 Madrid. Spain
Tel. +34 91 196 4552/ +34 91 196 4582
Fax. +34 91 196 4420
e-mail: jjlucas@cbm.uam.es
http://www.cbm.uam.es/lineas/lucasgroup.htm
http://www.ciberned.es/grupojoselucas.aspx

ABSTRACT

Huntington's disease (HD) is the most common of nine inherited neurological disorders caused by expanded-polyglutamine (polyQ) sequences which confer propensity to self-aggregate and toxicity to their corresponding mutant-proteins. It has been postulated that polyQ-expression compromises the folding capacity of the cell which might affect other misfolding prone proteins. α-Synuclein (α-syn) is a small neural-specific protein with propensity to self-aggregate that forms Parkinson's disease (PD) Lewy bodies. Point mutations in α-syn that favor self-aggregation or α-syn gene duplications lead to familial-PD, thus indicating that increased α-syn aggregation or levels are sufficient to induce neurodegeneration. Since polyQ-inclusions in HD and other polyQ-disorders are immunopositive for α-syn, we speculated that α-syn might be recruited as an additional mediator of polyQ-toxicity. Here we confirm in HD postmortem brains and in the R6/1 mouse model of HD the accumulation of α-syn in polyQ-inclusions. By isolating the characteristic filaments formed by aggregation prone proteins, we found that N-terminal mutant huntingtin (N-mutHtt) and α-syn form independent filamentous microaggregates in R6/1 mouse brain as well as in the inducible HD94 mouse model, and that N-mutHtt expression increases the load of α-syn filaments. Accordingly, α-syn knock-out results in diminished number of N-mutHtt inclusions in transfected neurons and also *in vivo* in the brain of HD mice. Finally, α-syn knock-out attenuates body-weight loss and early motor phenotype of HD mice. This study therefore demonstrates that α-syn is a modifier of polyQ-toxicity *in vivo* and raises the possibility that potential PD-related therapies aimed to counteract α-syn-toxicity might help to slow HD.

INTRODUCTION

Huntington's disease (HD) is the most common of a group of nine inherited devastating neurological disorders caused by CAG triplet-repeat expansions encoding expanded polyglutamine (polyQ) sequences which in turn confer toxicity to their mutated protein products (1). In HD, this expanded polyQ stretch is located in the N-terminal portion of the huntingtin (Htt) protein (2). A shared feature of polyQ diseases is the presence of nuclear and cytoplasmic intraneuronal inclusion bodies consisting primarily of aggregation-prone polyQ proteins (3, 4). The exact mechanism by which expanded polyQ induces neurodegeneration remains unknown. However, it has been suggested that progressive disruption of protein folding machinery of the cell might explain the commonalities among the neurodegenerative diseases associated with chronic expression of misfolded and aggregation prone-proteins (5).

α-Synuclein (α-syn) is a small neural-specific protein involved in synaptic function (6, 7) with propensity to self-aggregate (8). α-Syn has been implicated in the etiology of Parkinson's disease (PD) as well as of other neurodegenerative diseases such as multiple system atrophy and Lewy body dementia that share the presence of the characteristic cytoplasmic inclusions termed Lewy bodies (9). The notion of α-syn as a pathogenic protein arises from, in one hand, the fact that α-syn is the main component of Lewy bodies (9, 10) . On the other hand, point mutations in α-syn that confer a higher propensity for self-aggregation (11, 12) are linked to autosomal-dominant forms of PD (13-15) and duplication and triplication of the α-syn gene lead to a severe and highly

penetrant form of PD (16). Collectively, these findings highlight the ability α-syn to induce or cause neurodegeneration.

It has been reported that α-syn can also be detected in the inclusions of HD patients (17) and of patients of other CAG repeat disorders such as SCA-2 and SCA-3 (18, 19). The same holds true for the inclusions of the HD89 mouse model of HD (17). Furthermore, there is evidence that α-syn may act as a modifier of polyQ toxicity in cell and Drosophila models of HD. Namely, α-syn overexpression promotes aggregation of mutant Htt in PC12 and SKNSH neuroblastoma cells (20, 21), and neuronal expression of α-syn increases neurodegeneration of flies expressing exon-1 Q120 Htt in eyes (21).

Given the well-established pathogenicity of α-syn alterations, the accumulation of α-syn in inclusions of HD mice and patients and the crosstalk between α-syn and mutant Htt in cell and fly HD models, we reasoned that in the context of mutant Htt-induced disease, α-syn might be recruited as an additional mediator of toxicity. Here we aim to take advantage of mouse genetics to explore this. Accordingly, here we first confirm the presence of α-syn in cytoplasmic inclusions in brain of HD patients and extend this finding to the commonly used R6/1 mouse model of HD (22). Then, by applying a previously reported method (23) to isolate from mouse brain the filaments made of aggregation prone proteins, here we also explore whether N-mutHtt and α-syn co-aggregate within the same filamentous microaggregates or whether they instead form independent microaggregates. Finally, to decipher to which extent α-syn might contribute to polyQ induced toxicity, we here combine R6/1 N-mutHtt mice with α-syn knock-out mice (24) and subject them to behavioral and histopathological analysis.

RESULTS

Huntingtin and α-synuclein co-localize in inclusions of HD patients.

In agreement with a previous report (17), by performing immunohistochemistry with anti-α-syn antibodies on postmortem brain tissue from three grade 4 HD patients and three control subjects, we observed α-syn-positive inclusions in the striatum of patients and extended this finding to the cerebral cortex (Fig. 1A-D). As shown in Figure 1A, control subjects show a diffuse nerve terminal pattern while HD subjects also show abundant bead-like neuropil inclusions (see solid black arrows in Fig. 1B-C). Less frequently, α-syn immunoreactivity could also be detected in larger cytoplasmic perinuclear inclusions (see empty arrow in Fig. 1C) and, very rarely, in small intranuclear inclusions (see thin black arrow in Fig. 1D). We then performed double immunofluorescence to explore whether α-syn-positive inclusions coincide with Htt-positive inclusions. As shown in Figure 1E-J, α-syn-positive inclusions represent a fraction of the N-mutHtt-positive inclusions in neuropil and dystrophic neurites of HD brains. More precisely, 21% of the Htt-positive inclusions with diameter > 2.5 μm and 8% of the Htt-positive inclusions with diameter < 2.5 μm were also positive for α-syn. Furthermore, co-localization with α-syn was also observed when the detection of inclusions in HD brain was performed with an anti-ubiquitin antibody (data not shown).

α-synuclein is detected in inclusion bodies of HD mouse models, but forms independent filamentous microaggregates.

Mouse genetics can be a powerful tool to explore the relevance of α-syn to the pathogenesis of polyglutamine disease. Accordingly, we decided to test whether α-syn could be detected in inclusions of a commonly used mouse model of HD, namely, the R6/1 mouse line. These mice express N-mutHtt with a 116 CAG repeat and they show

abundant inclusions in striatal and cortical neurons as well as in other brain regions and develop a progressive HD-like behavioral phenotype (22). Immunohistochemistry with anti-α-syn antibodies in the brain of R6/1 mice revealed, apart from the widespread nerve terminal staining, the presence of some cytoplasmic or neuropil α-syn-positive inclusions (Fig. 2A). This is in agreement with a previous study performed on a mouse model expressing full length mutant Htt (17). However, α-syn-positive inclusions in the brain of R6/1 mice were rare in comparison to those found in human HD brain. By performing double immunofluorescence experiments we then confirmed that α-syn-positive inclusions in the brain of R6/1 mice are a subset of the Htt-positive neuropil inclusions (Fig. 2B). Similar results were obtained when the inclusions in R6/1 brains were labeled with an anti-ubiquitin antibody (Fig. 2C).

As exemplified in Figure 2D and in Supplementary figure 1, Htt inclusions in human (25), and mouse (23, 26) brain tissue are ultrastructurally composed of filamentous material. Both N-mutHtt and α-syn are known to aggregate following the classic amyloidogenic cascade from soluble oligomers to filamentous microaggregates (8, 27-30). We have previously reported a method for the isolation of such filamentous aggregates from the brain of HD mouse models (23). In view of the co-localization of N-mutHtt and α-syn in inclusions of R6/1 mice, we wondered whether N-mutHtt and α-syn would be co-aggregated in the same filaments. To explore this, we performed filament preparations from R6/1 mice and subjected them to double immuno-electron microscopy with anti-N-mutHtt and anti-α-syn antibodies. As shown in Figure 2E-F, the prominent N-mutHtt-positive filaments obtained from R6/1 mice were not immuno-decorated with the anti-α-syn antibody. The same result was obtained when the filament extraction was performed from brain tissue from a different HD mouse model, namely

the inducible HD94 mouse line (Fig. 2G-K). In both R6/1 and HD94 mice, the α-syn antibody decorated independent and smaller filaments (Fig. 2F, I-K). To further explore this and to verify the specificity of the α-syn immunodecoration, we performed filament preparations from R6/1 mice and, in parallel, also from wild type and α-syn knock-out mice as controls. Interestingly, analysis of the corresponding fractions from wild type mice revealed the presence of the same type of anti-α-syn-decorated filaments (Fig. 2L), although they were much less abundant than in the R6/1 samples (Fig. 2M; see quantification in Fig. 2N). The specificity of the detection of α-syn-decorated filaments was evidenced by their absence in samples from α-syn knock-out mice (Fig. 2N). In summary, apart from Htt-positive filaments, independent α-syn-positive filaments were observed in samples from R6/1 and HD94 mice. These α-syn-positive filaments were not exclusive of mice expressing mutant Htt, as they can also be observed in wild type mouse samples. However, they are much more abundant in N-mutHtt expressing mice. Therefore, since α-syn could not be detected in the Htt filaments obtained from HD mouse samples while it was found in different shorter filaments, we conclude that α-syn and N-mutHtt form independent filamentous microaggregates *in vivo*. Thus arguing against mixed cross-seeding and suggesting that α-syn and N-mutHtt co-localization in certain inclusions probably reflects the coalescence of independent homomeric microaggregates into the same inclusion bodies.

α-synuclein knock-out results in decreased number of Htt inclusions in exon1-HttQ72 transfected neurons and in R6/1 mice.

Since it was formerly described that α-syn overexpression promoted Htt aggregation in cellular models of HD (20, 21), we wondered whether α-syn deficiency would affect in the opposite manner the formation of N-mutHtt inclusions in a cell model. For this, we

performed striatal primary cultures from wild type (Wt) and α-syn knock-out (α-Syn-/-) mice and transfected them with exon 1-Htt with 17 (Q17) or 72 (Q72) CAG repeats each coupled to the enhanced green fluorescent protein (EGFP). After 16 h of transfection with Q17-EGFP, Wt and α-Syn-/- cells showed an even distribution of Q17-EGFP green fluorescence all over the cytoplasm (data not shown). Transfection with Q72-EGFP resulted in inclusion formations and yielded differences between Wt and α-Syn-/- cells (Fig. 3A). Interestingly, the percentage of transfected cells with diffuse fluorescence and no inclusions was significantly higher in Q72-EGFP α-Syn-/- cultures than in Q72-EGFP Wt cells (70.77±2.33% *vs.* 50.19±1.7%; *P*=0.002), as shown in histograms in Figure 3B-C. Inclusion counting was done considering two types of inclusions depending on whether they were smaller or bigger than 3.5 μm in diameter. Interestingly, Q72-EGFP α-Syn-/- cells presented less inclusions of the highest size than Q72-EGFP Wt cells (26.09±2.88% *vs.* 46.32±2.01%; *P*=0.005).

In view of these results, we decided to explore the effect of the lack of α-syn on the load of inclusions *in vivo* in a mouse model of HD. For this, we produced a small group of R6/1 mice in α-syn knock-out background by breeding with mice with a targeted deletion of the α-syn gene (24) and analyzed the number of Htt-positive inclusions at symptomatic ages. Sagittal brain sections of 8-month old R6/1 and R6/1;α-Syn-/- mice were immunostained with anti-N-terminal-Htt antibody. Htt-positive inclusions were abundant in the striatum of R6/1 mice at this age (Fig. 3D) and we quantified the number of inclusions with diameter higher than 6 μm. In good agreement with the results from primary transfected neurons, the number of striatal inclusions was lower in R6/1 mice with null α-syn gene dosage (R6/1 *vs.* R6/1;α-Syn-/-: 2138.80±177.73 inclusions/mm^2 *vs.* 1626.53±100.80 inclusions/mm^2; *P*=0.015) (Fig. 3E). However, this

decrease in the number of inclusions seems to occur only at late stages of R6/1 mice since it was not apparent in mice analyzed at the age of 5 months (data not shown). In summary, these results indicate that α-syn deficiency results in diminished number of N-mutHtt inclusions, not only in transfected primary neurons, but also *in vivo* in the brain of HD transgenic mice.

We then investigated whether the decrease in the number of inclusions observed in the striatum of 8-month old R6/1;α-Syn-/- mice correlated with changes in the proteolytic machinery of the cell. For this, we performed western blot analysis of proteins indicative of the status of the ubiquitin proteasome system (UPS) or the autophagy in the striatum of 8-month old R6/1;α-Syn-/- mice. As shown in Figure 3F, the poly-ubiquitin smears previously reported to be increased in R6 mice respect to wild type mice (31) were not significantly affected by the absence of α-syn. Thus suggesting that the decrease in the number of inclusions observed in R6/1;α-Syn-/- mice is not due to a different status of the UPS. Regarding autophagy, we measured by Western blot the levels of beclin-1 and of Atg5-Atg12 that are proteins involved in early and late stages of autophagy, respectively (Fig. 3G). Beclin-1 levels in R6/1 mice were unaffected by the knock-out of α-syn. However, the level of the Atg5-Atg12 complex shows a tendency to increase in R6/1 mice as the α-syn gene dosage decreases. Thus suggesting a facilitation of late stages of autophagy by α-syn knock-out. This might in part explain the decrease in the number of inclusions observed in R6/1;α-Syn-/- mice and fits well with the previous report of excess α-synuclein acting as a negative regulator of autophagy (21).

Analysis of the effect of α-synuclein-deficiency on the apoptosis and atrophy observed in striatum of R6/1 mice

We wondered if the decrease in Htt-positive inclusions in R6/1 mice in α-syn knock-out background would correlate with changes in other histopathological HD hallmarks, such as cell death or striatal atrophy. To test whether reduction in the number of inclusions correlates with differences in the rate of striatal apoptotic cell death observed at late stages of disease in R6/1 mice, we performed immunohistochemistry for cleaved caspase-3. Representative images in Figure 4A show the presence of positive cells for cleaved caspase-3 immunostaining in striatum at 8 months of age. As shown in histogram in Figure 4A, the number of cleaved caspase-3 cells in R6/1; α-Syn-/- mice presented a tendency to be lower than that in R6/1 mice and comparable to that observed in wild type mice. Similar results were obtained when the rate of apoptosis was analyzed by TUNEL staining (Fig. 4B). We then analyzed striatal volume in sagittal sections of transgenic mice by using the Cavalieri method. As seen in the histogram in Figure 4C, 8 month old R6/1 mice presented atrophy within the range of what has been described before (32), but this was not affected by the gene dosage of α-syn as it was homogeneous within the R6/1, R6/1;α-Syn+/- and R6/1;α-Syn-/- groups.

α-synuclein deficiency does not affect lifespan but attenuates body weight loss in R6/1 mice

In view of the results concerning inclusion load and incidence of apoptosis obtained in the first group of R6/1 mice in α-syn knock-out background, we decided to produce a bigger experimental group of mice for behavioral studies to explore whether α-syn is a relevant player in N-mutHtt-induced disease *in vivo*. This approach is favored by the fact that α-syn gene knock-out mice do not show any obvious behavioral abnormality

per se (24). By combining R6/1 mice and α-syn knock-out mice, we therefore obtained mice with any of the six following experimental genotypes: wild type mice (Wt), mice with an heterozygous deletion of the α-syn locus (α-Syn+/-), mice with an homozygous deletion of the α-syn locus (α-Syn-/-), mice that express N-mutHtt with normal α-syn alleles (R6/1), mice that express N-mutHtt with an heterozygous deletion of the α-syn locus (R6/1;α-Syn+/-) and mice that express N-mutHtt with an homozygous deletion of the α-syn locus (R6/1;α-Syn-/-). The breeding protocol starting with R6/1 and α-Syn-/- mice is shown in Supplementary figure 2A. Briefly, R6/1 male mice were crossed with α-Syn-/- female mice. Then, R6/1;α-Syn+/- and α-Syn+/- mice from the resulting offspring were intercrossed to obtain the six mentioned experimental genotypes (Suppl. Fig. 2B). This way, a total of 264 mice were generated that showed a normal mendelian segregation among the six possible genotypes, as confirmed by chi-square analysis (Suppl. Fig. 2C; P=0.414), thus indicating no embryonic lethality associated to any of the possible genotypes.

As a global indicator of the potential effect of α-syn gene dosage on polyQ-induced disease *in vivo*, life expectancy was monitored in these mice. Figure 5A shows the cumulative survival for the six genotypes calculated by means of the Kaplan-Meier analysis. Obviously, as previously reported, significant differences in lifespan were observed between non-N-mutHtt-expressing and N-mutHtt-expressing mice ($p_{Log\ Rank} \leq 0.0005$, $p_{Breslow} \leq 0.0005$, $p_{Tarone\text{-}Ware} \leq 0.0005$). However, there were no significant differences among N-mutHtt-expressing mice regarding survival. Lifespan for R6/1 mice was 297.37±10.28 days, for R6/1;α-Syn+/- mice was 289.00±9.66 days and for R6/1;α-Syn-/- mice was 289.35±10.26 days.

As an additional global indicator of the potential effect of α-syn gene dosage on polyQ-induced disease *in vivo* body weight was monitored along the whole study. As extensively reported (22, 33-35), R6/1 mice failed to show the progressive weight gain that wild type mice experience from 2.5 to 8 months of age. Figure 5B shows body weight evolution along time of the six genotypes expressed as percentage respect to Wt mice. N-mutHtt-expressing mice presented differences respect to Wt mice since early ages in the study. However, these differences did not appear at the same time in the three R6/1 groups. Thus, whereas R6/1 and R6/1;α-Syn+/- mice showed a decrease in body weight with respect to Wt mice at 2.5 months (Wt *vs.* R6/1: 100±1.51% *vs.* 82.41±2.78%, P=0.019; Wt *vs.* R6/1;α-Syn+/-: 100±1.51% *vs.* 90.74±1.54%, P=0.009), in the case of R6/1;α-Syn-/- mice the difference was not seen until the age of 4 months (Wt *vs.* R6/1;α-Syn-/-: 100±4.77% *vs.* 81.64±3.04%, P=0.023). In fact, as shown in Figure 5C-D body weight of R6/1;α-Syn-/- mice was almost 20% higher than that of R6/1 at 2.5 and 4 months (2.5 months: P=0.004; 4 months: $P\leq0.0005$) and milder but significant differences were maintained along the whole study. In summary, α-syn knock-out delays body weight deficit in R6/1 from 2.5 to 4 months of age and keeps attenuating it up to more advanced stages of disease progression.

α-synuclein deficiency attenuates early motor impairment in R6/1 mice

We then assessed the potential role of α-syn in mediating the motor phenotype of R6/1 mice. Scoring of clasping in the tail suspension test is a common assay to evaluate involuntary movements in HD mouse models (22, 36). Accordingly, mice were recorded for 30 s and the videos were stopped every 2 s to score each mouse and we analyzed the cumulative percentage of mice showing clasping. Since no gender differences were detected, male and female mice were grouped together for analysis of

genotype effect (Fig. 6A). Only N-mut-Htt-expressing mice showed clasping phenotype along the whole study starting at the age of 4 months. At this age, 60% of the R6/1 mice presented clasping phenotype. In contrast, only 33.3% and 28.5 % of R6/1;α-Syn+/- and R6/1;α-Syn-/- mice respectively showed clasping ($P \leq 0.005$). However, this beneficial effect of α-syn deficiency occurs only at initial stages of disease progression as the three R6/1 groups presented a similar percentage of clasping phenotype at 6 and 8 months of age.

Other common motor test widely used to examine HD mouse models is rotarod. It has been recently described that accelerating rotarod is more sensitive than fixed-speed rotarod for detecting early motor deficits in R6 mice (37). Thus, mice were analyzed on the rotarod apparatus set to accelerate from 4 to 40 rpm along a 5 min period and mice were tested in four trials with 1 h inter-trial periods. Mice were examined at the age of 2.5, 4, 6 and 8 months. Since no gender differences were detected, male and female mice were grouped together for analysis of genotype effect. As expected, N-mutHtt-expressing mice showed a deficit in this motor coordination task (Fig. 6B). This deficit started at the age of 4 months and then showed a progressive worsening until the last time point of the study, at 8 months. Interestingly, analysis of the percentage of mice on rod at the highest speeds of the accelerating paradigm (Fig. 6C) revealed that R6/1;α-Syn+/- and R6/1;α-Syn-/- mice perform better than R6/1 mice at 4 and 6 months of age (4 months, 36 rpm: $P=0.048$; 4 months, 40 rpm: $P=0.005$; 6 months, 32 rpm: $P=0.003$; 6 months, 36 and 40 rpm: $P=0.001$). In conclusion, analysis of clasping phenotype and rotarod performance revealed that α-syn deficiency attenuates motor phenotype of R6/1 mice at early stages of disease progression.

DISCUSSION

Increased levels or aggregation of α-syn are sufficient to induce neurodegeneration as evidenced by the facts that duplication or triplication of the α-syn gene or point mutations that confer a higher propensity for α-syn self-aggregation leads to severe forms of PD (13, 14, 16). Here we have confirmed in HD postmortem brains and in the R6/1 mouse model of HD the accumulation of α-syn in polyQ-inclusions that had been previously reported in patients of HD and other CAG repeat disorders (17-19). Furthermore, based on a method that we previously established to isolate filamentous microaggregates like those that form inclusion bodies (23), we here demonstrate that N-mutHtt and α-syn form independent homomeric filaments and that N-mutHtt expression increases the load of α-syn filamentous microaggregates. Thus, arguing against mixed cross-seeding and rather fitting with the suggested N-mutHtt-induced progressive disruption of cellular protein folding (5, 38), leading to homomeric aggregation of misfolding-prone proteins and subsequent coalescence of independent homomeric microaggregates into the same inclusion bodies. Finally, to explore whether α-syn is a modifier of polyQ-induced toxicity *in vivo* we took advantage of mouse genetics and found that α-syn knock-out results in diminished number of N-mutHtt inclusions in transfected mouse neurons and also *in vivo* in the brain of HD transgenic mice. Most importantly, α-syn knock-out also results in attenuation of the body weight-loss and of the early motor phenotype of HD mice.

Since α-syn knock-out *per se* does not induce a clear neurological phenotype in mice (24), combination of an HD mouse model and α-syn knock-out mice represents a powerful approach to decipher whether polyQ-induced alterations in α-syn proteostasis

might contribute to HD pathogenesis. The fact that α-syn deficiency attenuates body weight loss and early motor dysfunction of R6/1 mice strongly indicates that α-syn acts as an additional mediator of toxicity in early stages of polyQ-induced disease *in vivo*. The also reported effect of α-syn deficiency on the load of inclusion bodies suggests that competition for the protein folding machinery and/or interfering with protein degrading systems such as autophagy and the ubiquitin-proteasome system (UPS) might account for the recruitment of α-syn as an additional mediator of polyQ toxicity. Collectively, out data demonstrate that α-syn is a modifier of polyQ-induced toxicity *in vivo* and we will discuss below the possible underlying mechanisms.

Regarding the possible competition for the protein folding machinery, it has been shown that expression of expanded polyQ in various *C. elegans* strains expressing temperature sensitive mutants of structurally and functionally unrelated proteins results, at permissive temperatures, in induction of the phenotype associated with the aberrant conformation (5). Thus, suggesting that polyQ expression induces a progressive disruption of the folding capacity of the cell. Since there are many marginally stable or folding-defective proteins in the cell that may be affected by such disruption in the folding machinery, this has been postulated as a feedback mechanism that might explain the similarities among the many conformational neurodegenerative diseases (5). Our study suggests that α-syn may be one of such folding-defective proteins affected by N-mutHtt expression *in vivo*. N-mutHtt-induced alterations in α-syn conformation and aggregation could then significantly contribute to disease progression in the early stages but, as additional conformationally unstable proteins are engaged, the contribution of α-syn might become marginal thus explaining why α-syn knock-out does not significantly influence lifespan and late motor phenotype of R6/1 mice.

Regarding protein degradation, α-syn has been reported to be degraded mainly through autophagy (39). However, it has also been reported that proteasome inhibitor administration to cell models of polyQ disease results in increased formation of inclusion bodies and that these are immuno-positive for α-syn (40) and it is well documented that UPS and autophagy alterations affect each other, probably as compensatory mechanisms (41).

Whether the UPS is impaired in polyQ disease has been a matter of debate. On one hand, impaired proteasome activity was reported in polyQ cell models (42, 43) and we have also shown that filamentous microaggregates of N-mutHtt are able to impair 26S proteasome activity *in vitro* (44). On the contrary, proteasome activity was not diminished in brain homogenates of HD mice (45) and no global impairment of the UPS is detected under steady state expression of N-mutHtt in adult HD mice (31, 46, 47) despite accumulation of high molecular weight poly-ubiquitin conjugates (31). However, UPS impairment has been confirmed *in vivo* in mouse models but only locally at the synapse (48) or transiently upon acute N-mutHtt expression before inclusion formation takes place (47). In fact, such transient nature of polyQ-induced UPS impairment might also explain the transient beneficial effect of α-syn knock-out in early disease progression of R6/1 mice. α-Syn mediated toxicity might occur only transiently due to a recovery of the UPS upon efficient inclusion body formation. Regarding possible differences in the status of the UPS to account for the decrease in the number of inclusions observed in the striatum of 8-month old R6/1;α-Syn-/- mice, the here reported data of poly-ubiquitin smears not being significantly affected by the absence of α-syn argues against this possibility.

Regarding autophagy, here we show that the level of the Atg5-Atg12 complex shows a tendency to increase in R6/1 mice as the α-syn gene dosage decreases. This suggests a possible increase in autophagy that might in part explain the decrease in the number of inclusions observed in 8-month old R6/1;αSyn-/- mice and fits with the recent reports of α-syn as a negative regulator of autophagy. On one hand, excess α-syn has been shown to impair macroautophagy via Rab1a inhibition (21). Consequently, excess α-syn results in increased load of aggregates in cell models expressing exon-1 Q74 Htt and in increased neurodegeneration in flies expressing exon-1 Q120 Htt in eyes (21). More recently, a positive feedback loop model of excess α-syn inducing lysosomal dysfunction has been proposed (49). More precisely, in the context of the clinical link between the lysosomal storage disorder Gaucher disease (GD) and PD, Mazulli et al. reported that GD-linked mutations in glucocerebrosidase (GCase) result in increased level of glucosylceramide that facilitate formation of α-syn oligomers. This, in turn, hampers vesicle transport between endoplasmic reticulum and the Golgi apparatus, the main trafficking route for GCase to reach the lysosome. Therefore, it is possible that N-mutHtt-induced alterations in α-syn conformation and aggregation might contribute to *in vivo* progression of HD in part by affecting lysosomal function and autophagy.

We are not the first to describe α-syn accumulation in neurodegenerative diseases other than the typical synucleinopathies such as PD or Lewy body disease. As already mentioned, this had been described for various PolyQ diseases (17-19) and, interestingly, also for Alzheimer´s disease (AD). Since AD patients also show the typical tau and Aβ depositions, this disease has been considered a "triple brain amyloidosis" (50) and there are many *in vivo* studies supporting that α-syn affects Aβ

and tau pathology. As examples of α-syn and tau interaction, a patient with the α-synA53T mutation, exhibited neurofibrillar tangle pathology in addition to Lewy bodies (51) and a small percentage of the M83 α-synA53T transgenic mouse line also exhibits tau inclusions (52). As an example of α-syn and Aβ interactions, double transgenic α-syn/amyloid precursor protein (APP) mice exhibit increased α-syn deposition *versus* single-transgenic mice (53).

It had also been hypothesized that Aβ, tau, and α-syn promote the aggregation of one another probably through a cross-seeding mechanism (52). In fact, *in vitro* aggregation studies revealed that co-incubation of α-syn and tau promotes their polymerization (52). However, in good agreement with our results showing isolation of independent α-syn and N-mutHtt filaments from brain of R6/1 mice, analysis of filaments formed *in vitro* by co-incubation of tau and α-syn also revealed that they were essentially independent homopolymers (52). Heteromeric cross-seeding appears to occur only among proteins with equivalent molecular structures due to sequence similarity. Accordingly, N-mutHtt has been reported to cross-seed and form mixed fibrillation only with Q/N rich proteins such as the RNA-binding protein TIA-1(54) and the NM domains of Sup35p (55). Since α-syn does not share such a sequence similarity with tau or with N-mutHtt, it is not surprising that Giasson and co-workers and we observed independent homomeric filaments. Therefore, the coincidence of N-mutHtt and α-syn in inclusions is most likely the consequence of coalescence of the specific filaments in bigger aggregates similar to what has been described in cellular models expressing polyQ fusion proteins (38).

In summary, here we have confirmed in postmortem HD brains and in the R6/1 mouse model the accumulation of α-syn in polyQ inclusions that was previously reported in

brains of patients of various CAG repeat disorders. Furthermore, we found that N-mutHtt and α-syn form independent homomeric filaments. Finally to elucidate if α-syn is recruited as an additional player in pathogenicity triggered by N-mutHtt, we brought R6/1 mice to α-syn deficient backgrounds. Since α-syn deficiency results in improvement of body weight and of motor tasks in early symptomatic mice, we conclude that α-syn is a modifier of polyQ toxicity *in vivo*. The observed effect on α-syn knock-out on N-mut-Htt inclusion formation suggests that competition for protein folding and degradation machineries may underlie the observed beneficial effects of α-syn knock-out. Finally, our study also raises the possibility that any PD-related new experimental approach aimed to counteract α-syn toxicity might also be used to slow HD progression.

MATERIALS AND METHODS

Human samples

Brain specimens used in this study were removed at autopsy from three HD and three age-matched controls following the protocols of nervous tissue donation approved by the local Ethical Committees of the Barcelona and Bellvitge brain banks. The post-mortem delay in tissue processing was between 4 and 15 h in both groups. The neuropathological examination in HD cases revealed a diagnosis of HD grade 4 following the criteria of Vonsattel (56), revised in (57).

Animals

R6/1 mice transgenic for the human exon 1 huntingtin gene, in the B6CBAF1/J background (22) were used. Special attention was paid in order not to use B6CBAF1 mice from Harlan at any production step, since C57B6 mice from Harlan are known to be natural mutants lacking α-syn (58). α-Syn knock-out (α-Syn-/-) mice (B6; 129X1-Snca^{tm1Rosl}/J;(24)) were purchased from Jackson Laboratories. To obtain R6/1 mice in α-syn+/- and α-syn-/- backgrounds, male R6/1 mice (R6/1) were crossed with α-Syn-/- females. From the offspring, a second cross was set with R6/1;α-Syn +/- male mice and α-Syn +/- females, to achieve six different genotypes which covered from null to two α-syn gene doses and the presence or absence of the R6/1 transgene (Supplementary Figure 2).

Mice were bred at Centro de Biología Molecular "Severo Ochoa" (Madrid, Spain). Four or five mice were housed per cage with food and water *ad libitum*. Mice were maintained in a temperature-controlled environment on a 12 h light/dark cycle with lights onset at 7:30 A.M. All experiments were performed in accordance with

institutional guidelines approved by the ethical committee of Consejo Superior de Investigaciones Científicas (CSIC).

Immunohistochemistry and immunofluorescence in human tissue

Immunohistochemistry: human cryoprotected sections, 30 µm thick, were pre-treated in boiling epitope unmasking solution (SSC, 150 mM NaCl and 15 mM sodium citrate, pH 7.0) for 8 min to unmask aggregated α-syn. After cooling the slices in distilled water, sections were washed twice in PBS and endogenous peroxidase activity was inactivated with H_2O_2 in methanol for 30 min at room temperature and then sections were incubated in blocking solution (1% BSA, 0.5% fetal bovine serum and 0.2% Triton X-100 in PBS) for 1 hour at room temperature . Then, sections were incubated with mouse anti-α-Syn primary antibody (Novocastra) overnight at 4ºC. After washing with PBS, sections were incubated with the secondary components of the Elite Vectastain kit (Vector Laboratories). Diaminobenzidine (Sigma) was used as peroxidase substrate and, once dried, sections were cover slipped with PermaFluor Aqueous Monting Medium (Thermo Scientific).

Immunofluorescence: human paraffin sections, 4 µm thick, were pre-treated with 5% formic acid for 3 min to unmask aggregated α-syn and then incubated in 10% fetal bovine serum diluted in PBS to avoid non-specific binding. Sections were incubated overnight at 4°C with a combination of two primary antibodies: anti-α-synuclein (aa 111-131, Chemicon) and anti-N-terminal Htt (MAB5374, Millipore) or anti-α-synuclein (C-20)-R (Santa Cruz Biotechnology) and anti-N-terminal Htt (MAB5374). After washing with PBS, the sections were incubated with secondary antibodies: anti-rabbit Alexa 546 and anti-mouse Alexa 488 (Molecular Probes, Carlsbad, CA, USA) or anti-rabbit Texas Red-X 587 and anti-mouse Oregon Green 488 (Invitrogen). Nuclei were

counterstained with DAPI (Calbiochem). Subsequently, the sections were mounted with Fluorescent Mounting Medium (Dako), sealed and dried overnight at 4°C. Sections were examined with a Leica TCS-SL confocal microscope. For inclusion counting, 20 fields were counted at 40x magnification in an Axioskop 2 plus upright microscope (Zeiss) connected to a Coolsnap FX color camera (Roper Scientific). Data were expressed as percentage of Htt inclusions positive for α-synuclein labeling.

Immunohistochemistry and immunofluorescence in mouse tissue

In each experiment, all mice were processed in parallel and samples have been treated identically. Briefly, mice were sacrificed by CO_2, and brains were removed and halved sagittally immediately after decapitation. Left hemispheres were processed for histology, fixed with 4% paraformaldehyde (PFA) in Sorensen´s phosphate buffer overnight at 4°C, and then were immersed in 30% sucrose in PBS for 48 h for cryoprotection. Next, samples were frozen in OCT (Optimal Cutting Temperature, Tissue-Tek) and stored at -80ºC until use. Sagittal sections (30 µm) were cut on a CM 1950 Ag Protect freezing microtome (Leica), and placed and stored in a solution containing 30% glycerol and 30% ethyleneglycol in 0.02 M monobasic phosphate buffer at pH 7.2 at -20 ºC. To detect α-syn aggregates by immunohistochemistry or by immunofluorescence, a previous epitope unmasking step was performed as above described for the human tissue staining.

Immunohistochemistry: For α-syn detection in mouse tissue sagittal sections were pre-treated by boiling in epitope unmasking solution (SSC) for 8 min. After cooling the slices in distilled water, sections were pretreated for 30 min in 1% H_2O_2/PBS, followed by 1 h in blocking solution and incubated overnight with primary antibodies: mouse anti-α-Syn-1 (BD Transduction Laboratories), mouse anti-N-terminal Htt (MAB5374,

Millipore) and rabbit anti-cleaved caspase-3 (Asp175) (Cell Signaling). Finally, the peroxidase activity was developed with the Elite Vectastain kit (Vector Laboratories) using diaminobenzidine (Sigma). Sections were cover slipped with PermaFluor Aqueous Monting Medium (Thermo Scientific). Digital images were capture with an Olympus Bx 51 microscope coupled to a Color View IIIu digital camera with 20x objective lens with the help of the Olympus Soft Imaging System.

Immunofluroscence: after the unmasking step in SSC, sagittal sections were incubated with 1% Triton X-100 in PBS and followed by blocking solution (1% BSA and 0.1% Triton X-100 in PBS). Sections were further incubated with two combinations of primary antibodies: mouse anti-N-terminal Htt (MAB5374, Millipore) and rabbit anti-α-Syn (C-20)-R (Santa Cruz Biotechnology) or with rabbit anti-ubiquitin (Dako) and mouse anti-α-Syn [4D6] (Abcam) at 4ºC overnight. As secondary antibodies, anti-mouse Oregon Green 488 and anti-rabbit Texas Red-X 587 or anti-rabbit Oregon Green 488 and anti-mouse Texas Red-X 587 (Invitrogen) were used. Nuclei were stained with DAPI (Calbiochem). Once air dried in darkness, sections were cover slipped with PermaFluor Aqueous Monting Medium (Thermo Scientific). Images were acquired with the vertical Axio Imager.M2 microscope using the LSM510 software (Carl Zeiss) with a 100x, 1.4 numerical aperture oil immersion objective or with the vertical Axioskop2 plus microscope using the Metavue 5.07 software (Universal Imaging) with a 63x, 1.4 numerical aperture oil immersion objective.

Huntingtin inclusions counting in mouse samples

Four spaced regularly sections of each mouse were immunostained for anti-N-terminal Htt (MAB 5374, Millipore). Digital images of striatal Htt inclusions were captured with an Olympus Bx 51 microscope, Color View IIIu digital camera with a 40x objective

lens with the help of the Olympus Soft Imaging System. The number and size of inclusions were determined using the ImageJ software with the *Analyze Particles* routine (size 2.89-14.45 μm^2, threshold 0-75, circularity 0.81-1.00). Data are represented as the mean ± SEM.

TUNEL assay

For each mouse, five regularly spaced sagittal sections spanning the whole striatum were processed according to the In Situ Cell Death Detection Kit protocol (POD, Roche). All analyses were performed in a blinded manner, and results were presented as the number of TUNEL-positive cells per 30-μm section.

Striatal volume analysis

Striatal volume was determined in every sixth sagittal section by using the Cavalieri method. Digital images were captured at a 2.5x magnification (Canon EOS 450D digital camera). Striatal area from 15 sections for each animal was calculated by means of the ImageJ software. Considering a separation of 180 μm between each section, total striatal volume of each mouse was calculated. Data are represented as the mean ± SEM.

Western blot

Mouse brains were quickly dissected on an ice-cold plate. Extracts for western blot analysis were prepared by homogenizing the striatum in ice-cold extraction buffer consisting of 20 mM HEPES pH 7.4, 100 mM NaCl, 20 mM NaF, 1% Triton X-100, 1 mM sodium orthovanadate, 5 mM EDTA, and protease inhibitors (2 mM PMSF, 10 μg/ml aprotinin, 10 μg/ml leupeptin and 10 μg/ml pepstatin). The samples were centrifuged at 15,000 x *g* for 20 min at 4°C. The resulting supernatant was collected and

protein content was determined by Bradford. Five micrograms of total protein were electrophoresed on 10% SDS-polyacrylamide gel and transferred to a nitrocellulose membrane. The following primary antibodies were used: anti-ubiquitin (clone FK2, Millipore), anti-beclin1 (Santa Cruz Biotechnology), anti-Atg5 (Millipore) and anti-β-actin (Sigma). The blots were incubated with the primary antibody at 4°C overnight in 5% non-fat dried milk followed by secondary polyclonal anti-mouse or anti-rabbit immunoglobulins conjugated with HRP (DAKO Cytomation) and ECL detection (Perkin Elmer).

Tissue processing for electron microscopy

For electron microscopy, immunostained vibratome sections were processed as previously described (59). Briefly, the sections were postfixed in 2% OsO_4 for 1 h, dehydrated, embedded in Araldite, and flat-mounted in Formvar-coated slides, using plastic coverslips. After polymerization, selected areas were photographed, trimmed, reembedded in Araldite, and resectioned at 1 μm. These semithin sections were rephotographed and resectioned in ultrathin sections. The ultrathin sections were observed in a Jeol electron microscope, without heavy metal staining to avoid artifactual precipitates.

Immunoelectron microscopy of purified filamentous microaggregates

Isolation of filamentous microaggregates from mouse brain tissue was performed as previously described (23). Briefly, forebrains were homogenized in buffer 1 (10 mM Tris, 1 mM EGTA, 0.8 M NaCl, 10% sucrose, 0.1% Triton X-100, and protease inhibitors) in a glass homogenizer. After centrifugation at 5,000 rpm (Sorvall SS34 rotor, Thermo Scientific) for 20 min, the supernatant S1 was saved, and pellet P1 was

homogenized in buffer 1 and centrifuged again. The supernatants S1 and S2 were combined, adjusted to 1% (w/v) *N*-lauroylsarcosine and 1% (v/v) β-mercaptoethanol, and incubated for 2 h at room temperature. After centrifugation at 50,000 rpm (TLA-100.3 rotor, Beckman Coulter) for 45 min, filament containing pellets were homogenized in buffer 2 (10 mM Tris, 1 mM EGTA, 0.8 M NaCl, 10% sucrose, and protease inhibitors), layered over a discontinuous sucrose gradient consisting of 50% sucrose and 20% sucrose in buffer 3 (10 mM Tris, 1mM EGTA, 0.8 M NaCl) and centrifuged for 2 h at 35,000 rpm (SW40 rotor, Beckman Coulter). The filament containing fraction was collected from the 20–50% interface and stored at -70°C until use.

Double immunoelectron microscopy was performed after adsorption of the filament containing fraction to electron microscopy carbon-coated grids. Samples were incubated with anti-N-terminal Htt MAB5374 (MAB5374, Millipore), anti-N-terminal Htt CAG53b (amino acids 1–118 with a 51 polyQ stretch, a kind gift from Dr. Wanker, Berlin, Germany) and anti-α-synuclein (C-20) (Santa Cruz Biotechnologies). Grids were then incubated with secondary gold-conjugated antibodies (Sigma). Finally, the samples were stained with 2% uranyl acetate. Transmission electron microscopy was performed in a Jeol (Peabody, MA) model 1200EX electron microscope operated at 100 kV. For α-syn filament counting, 7 grids for each condition were analyzed by counting 4 fields per grid at 25000 x magnification.

Primary neuron culture, transfection, immunofluorescence and inclusion counting

Primary neuronal cultures were prepared according to modifications of established procedures (60). Briefly, Wt or α-Syn knock-out pups were sacrificed at postnatal day 0. Striatal tissue was dissected and dissociated with the Papain Dissociation System

(Worthington). Striatal neurons were maintained in Neurobasal medium (Invitrogen) supplemented with 1% sodium pyruvate, 0.5 mM glutamine, 10% v/v horse serum, and 1% penicillin/streptomycin, and grown on 3 μg/ml laminin (Sigma) and 10 μg/ml poly-L-lysine coated chamber slides (μ-Slide for high quality microscopy, Ibidi). After 2 h of incubation, the culture medium was replaced with Neurobasal medium supplemented with 1% sodium pyruvate, 0.5 mM glutamine and 2% B27. Cells were maintained in 95% air/5% CO_2 in a humidified incubator at 37°C.

Transfection was performed 1 day after plating. Htt constructs comprised pEGFP-1 with the N-terminal fragment of Htt with 17 or 72 CAG repeats fused to the enhanced green fluorescence protein (EGFP) (kindly provided by Drs. Finkbeiner and Arrasate). Cells were transiently transfected with 1μg plasmid DNA and 3 μl Lipofectamine (Invitrogen) in 100 μl Neurobasal medium. The mixture was carefully (drop by drop) directly added to the medium (without antibiotics) and incubated for 2 h in 95% air/5% CO_2 in a humidified incubator at 37°C. Next, cells were washed three times with PBS and added to Neurobasal medium supplemented with 1% sodium pyruvate, 0.5mM glutamine, 2% B27, and 1% penicillin/streptomycin. Transfection efficiency was controlled by counting the number of transfected neurons corrected by the total number of neurons (a minimum of 300 cells were analyzed per experimental condition). Transfection efficiency was between 3% and 6% across all experiments.

After 16 h of transfection, cells were fixed with 2% PFA in Sorensen´s phosphate buffer for 10 min and washed twice with PBS prior fixation in 4% PFA for 10 min. Then, slices were washed again in PBS and nuclei were stained with DAPI (Calbiochem). Once air dried in darkness, sections were cover slipped with Fluorosave (Calbiochem).

For inclusion counting, 60 fields from a total of 8 slices for each condition were counted at a magnification of 63x in Axioskop 2 plus upright microscope (Zeiss) coupled to a Coolsnap FX color camera (Roper Scientific).

Behavioral tests

Survival. 134 mice were kept for survival. Life expectancy study was finished at day 700, 350 days after the last N-mutHtt expressing mouse died spontaneously. Results are represented as Kaplan-Meier curves.

Body Weight. Starting at 2.5 months, mice were weighed once a month. Results are represented as the mean ± SEM.

Behavioral testing started at 2.5 months and finished at 8 months, when transgenic mice presented several difficulties to perform the tasks. The number of mice used in this round of behavioral test was 91.

Clasping. Mice were suspended by the tail ~ 20 cm above the cage for 30 s and recorded. Every 2 s, the video was stopped and the number of limbs clasping was observed. For cumulative percentage of mice clasping, the first time the animal clasped was scored as positive and was not considered again. Results are represented as the cumulative percentage of mice with clasping phenotype.

Rota-rod. Motor coordination was tested on an accelerating rotarod apparatus (Ugo Basile). Initially, each mouse was trained for two days. In the first day, mice performed 4 trials (1 h intervals) at a fixed speed (4 rpm) for 60 s. In the second day, mice performed also 4 trials at a fixed speed at 8 rpm for 60 s. The third day, rotarod was set to accelerate from 4 to 40 rpm over 5 min and mice were tested four times (1 h intervals). During accelerating trials, the latency of each mouse to fall from the rotarod

was measured. Results are represented as the mean ± SEM of the latencies to fall in the four trials and as the percentage of mice on rod at the highest speeds.

Statistical Analysis

The normality of the data was tested by means of Shapiro-Wilk test. In view of the results, for non-parametric data, the following tests were applied for comparison of differences in several variables among genotypes: Mann-Whitney *U* test to compare α-syn filaments counting; Kruskal-Wallis *H* test followed by Mann-Whitney *U* test were used in the case of cleaved-caspase-3, TUNEL, striatal volume, body weight and mean latency on rod studies. For parametric data, differences in several variables among genotypes were analyzed by the following tests: independent two-sample Student´s *t* test was applied for inclusion counting in cell cultures and one-way ANOVA followed by Bonferroni *post hoc* test were used for striatal inclusion counting in R6/1 mice. Genotype frequencies, percentage of clasping mice and percentage of mice on rotarod were analyzed by means of chi-square test. Cumulative survival was analyzed by Logrank, Breslow and Tarone-Ware tests. A critical value for significance of $P<0.05$ was use throughout the study. The SPSS 17.0 software was used for statistical analysis.

FUNDING

This work was supported by the Spanish Ministry of Science/MEC/MCINN, CiberNed, Comunidad Autónoma de Madrid and Fundación Ramón Areces. C. T-Z acknowledges a "Juan de la Cierva" and Fundación Ramón Areces research contracts.

ACKNOWLEDGEMENTS

We thank Dr. M.R. Fernández-Fernández for critical reading of the manuscript, Dr. E. Iglesias-Gutiérrez for expert advice and helpful discussions regarding statistical analysis and the members of Lucas' lab for helpful suggestions. We also thank Dr. Owen Howard for style correction and Desireé Ruiz, Alicia Tomico and the Optical and Confocal Microscope and Electron Microscope Facilities from CBMSO for excellent technical assistance.

Conflict of Interest statement: None declared.

REFERENCES

1 Orr, H.T. and Zoghbi, H.Y. (2007) Trinucleotide repeat disorders. *Annu. Rev. Neurosci.*, **30**, 575-621.

2 Huntington's Disease Collaborative Research Group (1993) A novel gene containing a trinucleotide repeat that is expanded and unstable on Huntington's disease chromosomes. *Cell*, **72**, 971-983.

3 Ross, C.A. (1997) Intranuclear neuronal inclusions: a common pathogenic mechanism for glutamine-repeat neurodegenerative diseases? *Neuron*, **19**, 1147-1150.

4 Ross, C.A. and Poirier, M.A. (2004) Protein aggregation and neurodegenerative disease. *Nat. Med.*, **10 Suppl**, S10-17.

5 Gidalevitz, T., Ben-Zvi, A., Ho, K.H., Brignull, H.R. and Morimoto, R.I. (2006) Progressive disruption of cellular protein folding in models of polyglutamine diseases. *Science*, **311**, 1471-1474.

6 Chandra, S., Gallardo, G., Fernandez-Chacon, R., Schluter, O.M. and Sudhof, T.C. (2005) Alpha-synuclein cooperates with CSPalpha in preventing neurodegeneration. *Cell*, **123**, 383-396.

7 Burre, J., Sharma, M., Tsetsenis, T., Buchman, V., Etherton, M.R. and Sudhof, T.C. (2010) Alpha-synuclein promotes SNARE-complex assembly in vivo and in vitro. *Science*, **329**, 1663-1667.

8 Giasson, B.I., Uryu, K., Trojanowski, J.Q. and Lee, V.M. (1999) Mutant and wild type human alpha-synucleins assemble into elongated filaments with distinct morphologies in vitro. *J. Biol. Chem.*, **274**, 7619-7622.

9 Dickson, D.W. (2001) Alpha-synuclein and the Lewy body disorders. *Curr. Opin. Neurol.*, **14**, 423-432.

10 Spillantini, M.G., Crowther, R.A., Jakes, R., Hasegawa, M. and Goedert, M. (1998) alpha-Synuclein in filamentous inclusions of Lewy bodies from Parkinson's disease and dementia with lewy bodies. *Proc. Natl. Acad. Sci. U S A*, **95**, 6469-6473.

11 Conway, K.A., Harper, J.D. and Lansbury, P.T. (1998) Accelerated in vitro fibril formation by a mutant alpha-synuclein linked to early-onset Parkinson disease. *Nat. Med.*, **4**, 1318-1320.

12 Narhi, L., Wood, S.J., Steavenson, S., Jiang, Y., Wu, G.M., Anafi, D., Kaufman, S.A., Martin, F., Sitney, K., Denis, P. *et al.* (1999) Both familial Parkinson's disease mutations accelerate alpha-synuclein aggregation. *J. Biol. Chem.*, **274**, 9843-9846.

13 Polymeropoulos, M.H., Lavedan, C., Leroy, E., Ide, S.E., Dehejia, A., Dutra, A., Pike, B., Root, H., Rubenstein, J., Boyer, R. *et al.* (1997) Mutation in the alpha-synuclein gene identified in families with Parkinson's disease. *Science*, **276**, 2045-2047.

14 Kruger, R., Kuhn, W., Muller, T., Woitalla, D., Graeber, M., Kosel, S., Przuntek, H., Epplen, J.T., Schols, L. and Riess, O. (1998) Ala30Pro mutation in the gene encoding alpha-synuclein in Parkinson's disease. *Nat. Genet.*, **18**, 106-108.

15 Zarranz, J.J., Alegre, J., Gomez-Esteban, J.C., Lezcano, E., Ros, R., Ampuero, I., Vidal, L., Hoenicka, J., Rodriguez, O., Atares, B. *et al.* (2004) The new mutation, E46K, of alpha-synuclein causes Parkinson and Lewy body dementia. *Ann. Neurol.*, **55**, 164-173.

16 Singleton, A.B., Farrer, M., Johnson, J., Singleton, A., Hague, S., Kachergus, J., Hulihan, M., Peuralinna, T., Dutra, A., Nussbaum, R. *et al.* (2003) alpha-Synuclein locus triplication causes Parkinson's disease. *Science*, **302**, 841.

17 Charles, V., Mezey, E., Reddy, P.H., Dehejia, A., Young, T.A., Polymeropoulos, M.H., Brownstein, M.J. and Tagle, D.A. (2000) Alpha-synuclein immunoreactivity of

huntingtin polyglutamine aggregates in striatum and cortex of Huntington's disease patients and transgenic mouse models. *Neurosci. Lett.*, **289**, 29-32.
18 Alves, S., Regulier, E., Nascimento-Ferreira, I., Hassig, R., Dufour, N., Koeppen, A., Carvalho, A.L., Simoes, S., de Lima, M.C., Brouillet, E. *et al.* (2008) Striatal and nigral pathology in a lentiviral rat model of Machado-Joseph disease. *Hum. Mol. Genet.*, **17**, 2071-2083.
19 Berciano, J. and Ferrer, I. (2005) Glial cell cytoplasmic inclusions in SCA2 do not express alpha-synuclein. *J. Neurol.*, **252**, 742-744.
20 Furlong, R.A., Narain, Y., Rankin, J., Wyttenbach, A. and Rubinsztein, D.C. (2000) alpha-synuclein overexpression promotes aggregation of mutant huntingtin. *Biochem. J.*, **346 Pt 3**, 577-581.
21 Winslow, A.R., Chen, C.W., Corrochano, S., Acevedo-Arozena, A., Gordon, D.E., Peden, A.A., Lichtenberg, M., Menzies, F.M., Ravikumar, B., Imarisio, S. *et al.* (2010) alpha-Synuclein impairs macroautophagy: implications for Parkinson's disease. *J. Cell Biol.*, **190**, 1023-1037.
22 Mangiarini, L., Sathasivam, K., Seller, M., Cozens, B., Harper, A., Hetherington, C., Lawton, M., Trottier, Y., Lehrach, H., Davies, S.W. *et al.* (1996) Exon 1 of the HD gene with an expanded CAG repeat is sufficient to cause a progressive neurological phenotype in transgenic mice. *Cell*, **87**, 493-506.
23 Diaz-Hernandez, M., Moreno-Herrero, F., Gomez-Ramos, P., Moran, M.A., Ferrer, I., Baro, A.M., Avila, J., Hernandez, F. and Lucas, J.J. (2004) Biochemical, ultrastructural, and reversibility studies on huntingtin filaments isolated from mouse and human brain. *J. Neurosci.*, **24**, 9361-9371.
24 Abeliovich, A., Schmitz, Y., Farinas, I., Choi-Lundberg, D., Ho, W.H., Castillo, P.E., Shinsky, N., Verdugo, J.M., Armanini, M., Ryan, A. *et al.* (2000) Mice lacking alpha-synuclein display functional deficits in the nigrostriatal dopamine system. *Neuron*, **25**, 239-252.
25 DiFiglia, M., Sapp, E., Chase, K., Davies, S., Bates, G., Vonsattel, J. and Aronin, N. (1997) Aggregation of huntingtin in neuronal intranuclear inclusions and dystrophic neurites in brain. *Science*, **277**, 1990-1993.
26 Davies, S.W., Turmaine, M., Cozens, B.A., DiFiglia, M., Sharp, A.H., Ross, C.A., Scherzinger, E., Wanker, E.E., Mangiarini, L. and Bates, G.P. (1997) Formation of neuronal intranuclear inclusions underlies the neurological dysfunction in mice transgenic for the HD mutation. *Cell*, **90**, 537-548.
27 Poirier, M.A., Li, H., Macosko, J., Cai, S., Amzel, M. and Ross, C.A. (2002) Huntingtin spheroids and protofibrils as precursors in polyglutamine fibrilization. *J. Biol. Chem.*, **277**, 41032-41037.
28 Conway, K.A., Harper, J.D. and Lansbury, P.T., Jr. (2000) Fibrils formed in vitro from alpha-synuclein and two mutant forms linked to Parkinson's disease are typical amyloid. *Biochemistry*, **39**, 2552-2563.
29 Ross, C.A. and Poirier, M.A. (2005) Opinion: What is the role of protein aggregation in neurodegeneration? *Nature reviews*, **6**, 891-898.
30 Scherzinger, E., Sittler, A., Schweiger, K., Heiser, V., Lurz, R., Hasenbank, R., Bates, G.P., Lehrach, H. and Wanker, E.E. (1999) Self-assembly of polyglutamine-containing huntingtin fragments into amyloid-like fibrils: implications for Huntington's disease pathology. *Proc. Natl. Acad. Sci. U S A*, **96**, 4604-4609.
31 Maynard, C.J., Bottcher, C., Ortega, Z., Smith, R., Florea, B.I., Diaz-Hernandez, M., Brundin, P., Overkleeft, H.S., Li, J.Y., Lucas, J.J. *et al.* (2009) Accumulation of ubiquitin conjugates in a polyglutamine disease model occurs without global

ubiquitin/proteasome system impairment. *Proc. Natl. Acad. Sci. U S A*, **106**, 13986-13991.
32 Chopra, V., Fox, J.H., Lieberman, G., Dorsey, K., Matson, W., Waldmeier, P., Housman, D.E., Kazantsev, A., Young, A.B. and Hersch, S. (2007) A small-molecule therapeutic lead for Huntington's disease: preclinical pharmacology and efficacy of C2-8 in the R6/2 transgenic mouse. *Proc. Natl. Acad. Sci. U S A*, **104**, 16685-16689.
33 van Dellen, A., Blakemore, C., Deacon, R., York, D. and Hannan, A.J. (2000) Delaying the onset of Huntington's in mice. *Nature*, **404**, 721-722.
34 Naver, B., Stub, C., Moller, M., Fenger, K., Hansen, A.K., Hasholt, L. and Sorensen, S.A. (2003) Molecular and behavioral analysis of the R6/1 Huntington's disease transgenic mouse. *Neuroscience*, **122**, 1049-1057.
35 Rubio, I., Rodriguez-Navarro, J.A., Tomas-Zapico, C., Ruiz, C., Casarejos, M.J., Perucho, J., Gomez, A., Rodal, I., Lucas, J.J., Mena, M.A. *et al.* (2009) Effects of partial suppression of parkin on huntingtin mutant R6/1 mice. *Brain Res.*, **1281**, 91-100.
36 Yamamoto, A., Lucas, J.J. and Hen, R. (2000) Reversal of neuropathology and motor dysfunction in a conditional model of Huntington's disease. *Cell*, **101**, 57-66.
37 Pallier, P.N., Drew, C.J. and Morton, A.J. (2009) The detection and measurement of locomotor deficits in a transgenic mouse model of Huntington's disease are task- and protocol-dependent: influence of non-motor factors on locomotor function. *Brain Res. Bull.*, **78**, 347-355.
38 Rajan, R.S., Illing, M.E., Bence, N.F. and Kopito, R.R. (2001) Specificity in intracellular protein aggregation and inclusion body formation. *Proc. Natl. Acad. Sci. U S A*, **98**, 13060-13065.
39 Paxinou, E., Chen, Q., Weisse, M., Giasson, B.I., Norris, E.H., Rueter, S.M., Trojanowski, J.Q., Lee, V.M. and Ischiropoulos, H. (2001) Induction of alpha-synuclein aggregation by intracellular nitrative insult. *J. Neurosci.*, **21**, 8053-8061.
40 Waelter, S., Boeddrich, A., Lurz, R., Scherzinger, E., Lueder, G., Lehrach, H. and Wanker, E.E. (2001) Accumulation of mutant huntingtin fragments in aggresome-like inclusion bodies as a result of insufficient protein degradation. *Mol. Biol. Cell*, **12**, 1393-1407.
41 Lamark, T. and Johansen, T. (2010) Autophagy: links with the proteasome. *Curr. Opin. Cell Biol.*, **22**, 192-198.
42 Jana, N.R., Zemskov, E.A., Wang, G. and Nukina, N. (2001) Altered proteasomal function due to the expression of polyglutamine- expanded truncated N-terminal huntingtin induces apoptosis by caspase activation through mitochondrial cytochrome c release. *Hum. Mol. Genet.*, **10**, 1049-1059.
43 Bence, N.F., Sampat, R.M. and Kopito, R.R. (2001) Impairment of the ubiquitin-proteasome system by protein aggregation. *Science*, **292**, 1552-1555.
44 Diaz-Hernandez, M., Valera, A.G., Moran, M.A., Gomez-Ramos, P., Alvarez-Castelao, B., Castano, J.G., Hernandez, F. and Lucas, J.J. (2006) Inhibition of 26S proteasome activity by huntingtin filaments but not inclusion bodies isolated from mouse and human brain. *J. Neurochem.*, **98**, 1585-1596.
45 Diaz-Hernandez, M., Hernandez, F., Martin-Aparicio, E., Gomez-Ramos, P., Moran, M.A., Castano, J.G., Ferrer, I., Avila, J. and Lucas, J.J. (2003) Neuronal induction of the immunoproteasome in Huntington's disease. *J. Neurosci.*, **23**, 11653-11661.
46 Bett, J.S., Cook, C., Petrucelli, L. and Bates, G.P. (2009) The ubiquitin-proteasome reporter GFPu does not accumulate in neurons of the R6/2 transgenic mouse model of Huntington's disease. *PLoS One*, **4**, e5128.

47 Ortega, Z., Diaz-Hernandez, M., Maynard, C.J., Hernandez, F., Dantuma, N.P. and Lucas, J.J. (2010) Acute polyglutamine expression in inducible mouse model unravels ubiquitin/proteasome system impairment and permanent recovery attributable to aggregate formation. *J. Neurosci.*, **30**, 3675-3688.
48 Wang, J., Wang, C.E., Orr, A., Tydlacka, S., Li, S.H. and Li, X.J. (2008) Impaired ubiquitin-proteasome system activity in the synapses of Huntington's disease mice. *J. Cell Biol.*, **180**, 1177-1189.
49 Mazzulli, J.R., Xu, Y.H., Sun, Y., Knight, A.L., McLean, P.J., Caldwell, G.A., Sidransky, E., Grabowski, G.A. and Krainc, D. (2011) Gaucher Disease Glucocerebrosidase and alpha-Synuclein Form a Bidirectional Pathogenic Loop in Synucleinopathies. *Cell*, **146**, 37-52.
50 Trojanowski, J.Q. (2002) "Emerging Alzheimer's disease therapies: focusing on the future". *Neurobiol. Aging*, **23**, 985-990.
51 Duda, J.E., Giasson, B.I., Mabon, M.E., Miller, D.C., Golbe, L.I., Lee, V.M. and Trojanowski, J.Q. (2002) Concurrence of alpha-synuclein and tau brain pathology in the Contursi kindred. *Acta Neuropathol.*, **104**, 7-11.
52 Giasson, B.I., Forman, M.S., Higuchi, M., Golbe, L.I., Graves, C.L., Kotzbauer, P.T., Trojanowski, J.Q. and Lee, V.M. (2003) Initiation and synergistic fibrillization of tau and alpha-synuclein. *Science*, **300**, 636-640.
53 Masliah, E., Rockenstein, E., Veinbergs, I., Sagara, Y., Mallory, M., Hashimoto, M. and Mucke, L. (2001) beta-amyloid peptides enhance alpha-synuclein accumulation and neuronal deficits in a transgenic mouse model linking Alzheimer's disease and Parkinson's disease. *Proc. Natl. Acad. Sci. U S A*, **98**, 12245-12250.
54 Furukawa, Y., Kaneko, K., Matsumoto, G., Kurosawa, M. and Nukina, N. (2009) Cross-seeding fibrillation of Q/N-rich proteins offers new pathomechanism of polyglutamine diseases. *J. Neurosci.*, **29**, 5153-5162.
55 Krammer, C., Kremmer, E., Schatzl, H.M. and Vorberg, I. (2008) Dynamic interactions of Sup35p and PrP prion protein domains modulate aggregate nucleation and seeding. *Prion*, **2**, 99-106.
56 Vonsattel, J.P., Myers, R.H., Stevens, T.J., Ferrante, R.J., Bird, E.D. and Richardson, E.P., Jr. (1985) Neuropathological classification of Huntington's disease. *J Neuropathol. Exp. Neurol.*, **44**, 559-577.
57 Vonsattel, J.P. and DiFiglia, M. (1998) Huntington disease. *J. Neuropathol. Exp. Neurol.*, **57**, 369-384.
58 Specht, C.G. and Schoepfer, R. (2001) Deletion of the alpha-synuclein locus in a subpopulation of C57BL/6J inbred mice. *BMC Neurosci.*, **2**, 11.
59 Lucas, J.J., Hernandez, F., Gomez-Ramos, P., Moran, M.A., Hen, R. and Avila, J. (2001) Decreased nuclear beta-catenin, tau hyperphosphorylation and neurodegeneration in GSK-3beta conditional transgenic mice. *EMBO J.*, **20**, 27-39.
60 Martin-Aparicio, E., Yamamoto, A., Hernandez, F., Hen, R., Avila, J. and Lucas, J.J. (2001) Proteasomal-dependent aggregate reversal and absence of cell death in a conditional mouse model of Huntington's disease. *J. Neurosci.*, **21**, 8772-8781.

LEGENDS TO FIGURES

Figure 1: Huntingtin and α-synuclein co-localize in inclusions of HD postmortem human brain. α-synuclein immunohistochemistry in samples of human cerebral cortex of control subjects (**A**). or grade 4 HD patients (**B-D**). In the HD samples, α-synuclein immunoreactivity often appears as small inclusions in the neuropil (**B-C**, solid black arrows). It can also occasionally appear as large cytoplasmic perinuclear inclusions (empty arrow in **C**) and, exceptionally, as small intranuclear inclusions (thin black arrow in **D**). Double immunofluorescence staining of cortical sections from HD patients. Note that some N-mutHtt-positive cytoplasmic inclusions and dystrophic neurites (**E, H**; green fluorescence) were also labeled with α-syn antibody (**F, I**; red fluorescence), as shown in the merged image with DAPI nuclear counterstaining in blue (**G, J**).

Figure 2: α-synuclein is detected in Htt inclusion bodies of HD mouse models, but forms independent filamentous microaggregates. **A**, α-syn immunohistochemistry in cortex of R6/1 mice revealed the presence of bead-like neuropil inclusions (solid black arrow) similar to those seen in the human samples. **B**, Sections from R6/1 mice subjected to double Htt (green) and α-syn (red) immunofluorescence followed by DAPI blue nuclear counterstaining were analyzed under confocal microscope and revealed the presence of α-syn in a subset of N-mutHtt-positive cytoplasmic inclusions (white arrows). **C,** Double α-syn (red) and ubiquitin (green) immunofluorescence experiments were analyzed under a confocal microscope and revealed the presence of α-syn in a subset of neuropil ubiquitin-positive inclusion bodies (white arrow). **D**, Ultrastructural

transmission electron analysis of an N-mutHtt-stained neuropil inclusion in the striatum of an R6/1 mouse. White arrows indicate the filamentous ultrastructure of the aggregate. **E-M**, Immunoelectron microscopy analysis of filamentous aggregates isolated from the forebrain of HD mice. **E-F**, N-mutHtt-positive filaments from R6/1 mice (decorated with 5-nm gold particles, black arrows) were not co-decorated for α-syn (detected with 10 nm gold particles). **G-K**, Filamentous aggregates isolated from the forebrain of Tet/HD94 mice. As for R6/1 mice, N-mutHtt filaments (in this case decorated with 10-nm gold particles, black arrows) were not co-decorated for α-syn (detected with 5 nm gold particles). In both models, independent α-syn filaments were detected (**F, I, J** and **K**; empty arrows). Fractions from wild type mice showed the same type of anti-α-syn-decorated filaments (**L**), although R6/1 samples presented a higher number of anti-α-syn-decorated filaments (**M**) as seen in histogram in **N,** that represents α-syn filament counting in α-Syn-/-, Wt and R6/1 mice. Data are presented as mean ± SEM; *, $P < 0.05$. At least four animals per genotype were used.

Figure 3: **α-synuclein knock-out results in decreased number of Htt inclusions in exon1-HttQ72 transfected neurons and in R6/1 mice**. **A-C**, Primary striatal neuron cultures from Wt and α-Syn-/- mice were transfected with exon1-Htt-Q72-EGFP (Q72-GFP) which resulted in inclusion formation (**A**, white arrows). **B**, The 100% stacked column histogram shows the contribution of cells with inclusions to the total of the transfected cells in each genotype. **C**, Inclusion counting showed that, in Q72-GFP-transfected α-Syn-/- cells, the percentage of cells with inclusions higher than 3.5 μm was significantly lower than in the Wt cultures. A total of eight independent cultures were analyzed. **D-E**, N-mutHtt immunohistochemistry on brain sections from 8 month-old R6/1 mice with different α-syn dosage. **D**, Panels show representative images of the

striatum. **E**, Counting of aggregates with diameter higher than 6 μm. As in primary striatal neuronal cultures, the number of inclusions is lower in α-Syn-/- background. **F**, Western blot analysis of poly-ubiquitin smears. Histogram shows no significant differences among the three R6/1 genotypes with varying α-syn gene dosage. **G**, Western blot analysis of Beclin-1 and of the Atg5-Atg12 complex. Histogram shows no differences among the three R6/1 genotypes with varying α-syn gene dosage in Beclin-1 levels, while Atg5-Atg12 complex shows a tendency to increase in R6/1;α-Syn-/- mice respect to the other R6/1 mice. At least four animals per genotype were analyzed. Data are presented as mean ± SEM. *, $P < 0.05$; **, $P < 0.01$.

Figure 4: **Analysis of the effect of α-synuclein-deficiency on the apoptosis and atrophy observed in striatum of R6/1 mice. A**, Immunohistochemistry for cleaved caspase-3 on brain sections from 8 month old R6/1 mice with different α-syn gene dosage. Left panels show representative images of caspase-3 positive cells in the striatum (black arrows). R6/1;α-Syn-/- mice presented a tendency to fewer cells positive for caspase-3 (see histogram on the right), although it did not reach significance. **B**, TUNEL staining in R6/1 mice with different α-syn gene dosage. Left panels show representative image of TUNEL positive cells in the striatum (black arrows). As in the caspase-3 analysis, R6/1;α-Syn-/- mice presented a tendency to fewer TUNEL positive cells (see histogram on the right). **C**, Striatal Volume. Representative images of thionine stained sagittal sections of Wt and R6/1 mice at 8 months of age (striatal atrophy is observed in R6/1 sections). Histogram shows quantification of striatal volume. No differences were observed among R6/1 mice with different α-syn gene dosage. Results are expressed as mean ± SEM. At least three animals per genotype were analyzed.

Figure 5: α-synuclein deficiency does not affect lifespan, but attenuates body weight loss in R6/1 mice. A, Kaplan-Meier curve for cumulative survival. Lifespan is shown over a period of 700 days. Number of mice analyzed: Wt (12), α-Syn+/- (38), α-Syn-/- (23), R6/1 (19), R6/1;α-Syn+/- (43) and R6/1;α-Syn-/- (19). **B-D**, Body Weight. **B**, Histogram shows the percentage of body weight respect to Wt mice. a: Wt *vs.* R6/1: from 2.5 months onwards; b: Wt *vs.* R6/1;α-Syn+/-: from 2.5 months onwards; c: Wt *vs.* R6/1;α-Syn-/-: from 4 months onwards; d: α-Syn+/- *vs.* R6/1;α-Syn+/-: from 2.5 months onwards; e: α-Syn-/- *vs.* R6/1α-Syn-/-: from 5 months onwards; f: R6/1 *vs.* R6/1;α-Syn+/-: from 2.5 months onwards. **C**, Body weight of N-mutHtt expressing mice with different α-syn gene dosage at 2.5 and 4 months of age. **D**, Data from N-mutHtt expressing mice with varying gene dosage of α-syn were normalized respect to their non-N-mutHtt-transgenic counterparts (dashed line). Differences are seen later in the case of R6/1;α-Syn-/- mice, namely at 5 months of age (#: differences between non-N-mutHtt expressing mice *vs.* N-mutHtt expressing mice from this point onwards). Furthermore, R6/1;α-Syn-/- mice presented higher body weight compared to R6/1 mice at all ages (asterisks). Results are expressed as mean ± SEM; # $P < 0.05$, * $P < 0.05$, ** $P < 0.01$, *** $P < 0.001$. Number of mice analyzed: Wt (7), α-Syn+/- (18), α-Syn-/- (20), R6/1 (10), R6/1;α-Syn+/- (21) and R6/1;α-Syn-/- (14). C and D show only data from males while B shows both males and females.

Figure 6: **α-synuclein deficiency attenuates early motor impairment in R6/1 mice. A**, Cumulative percentage of mice showing clasping. The percentage of clasping mice is higher in R6/1 than in R6/1;α-Syn+/- and R6/1;α-Syn-/- groups at 4 months of age. After 6 months all N-mutHtt expressing mice presented a similar clasping phenotype.

Number of mice analyzed: R6/1 (10), R6/1;α-Syn+/- (19) and R6/1;α-Syn-/- (12). **B-C**, Rotarod. **B**, Evolution from 2.5 to 8 months of age of the mean latency to fall from rod. N-mutHtt expressing mice showed a deficit in motor performance from 4 month onwards in comparison to the non-N-mutHtt expressing mice (a). **C**, Percentage of N-mutHtt expressing mice remaining on rod at the highest speeds. At 4 and 6 months, the percentage of R6/1;α-Syn-/- animals able to reach the highest speeds (32, 36 and 40 rpm) is higher than in R6/1 mice. Number of mice analyzed: Wt (7), α-Syn+/- (18), α-Syn-/- (20), R6/1 (10), R6/1;α-Syn+/- (21) and R6/1;α-Syn-/- (14). Data are expressed as percentage over the total genotype population; *, $P < 0.05$; **, $P < 0.01$; ***, $P < 0.001$.

ABBREVIATIONS

AD: Alzheimer´s disease

HD: Huntington´s disease

Htt: Huntingtin

N-mutHtt: N-terminal-mutant huntingtin

PD: Parkinson´s disease

PolyQ: polyglutamine

α-Syn: α-Synuclein

UPS: ubiquitin proteasome system

SUPPLEMENTARY MATERIAL

Supplementary Figure 1: Immuno-electron microscopy image showing the filamentous ultrastructure of a small inclusion in cortex of a HD94 mouse stained with the CAG53b anti-N-terminal Htt antibody and developed with a secondary antibody conjugated to peroxidase. Thick arrows show filaments with a strong DAB precipitate labeling. Magnification: 60000 x.

Supplementary Figure 2: Breeding Protocol. **A**, Schematic representation of the breeding protocol to obtain R6/1 mice with decreased α-syn gene dosage. **B**, Number of experimental mice obtained for the whole study. **C**, Frequencies of the observed and the expected number of animals for each genotype is shown.

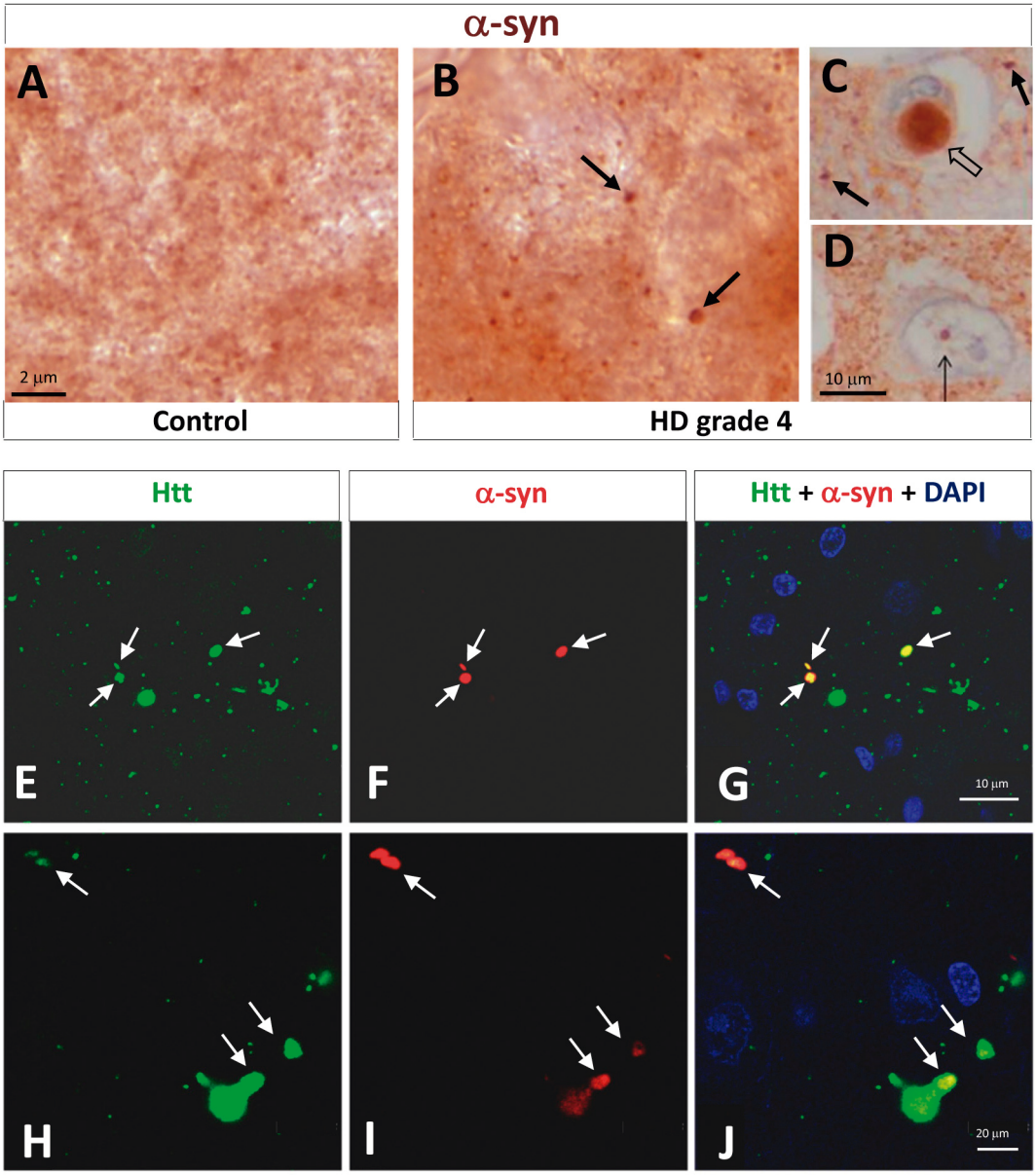
α-syn
A
B
C
D
2 µm
10 µm
Control
HD grade 4
Htt
α-syn
Htt + α-syn + DAPI
E
F
G
10 µm
H
I
J
20 µm

Figure 1

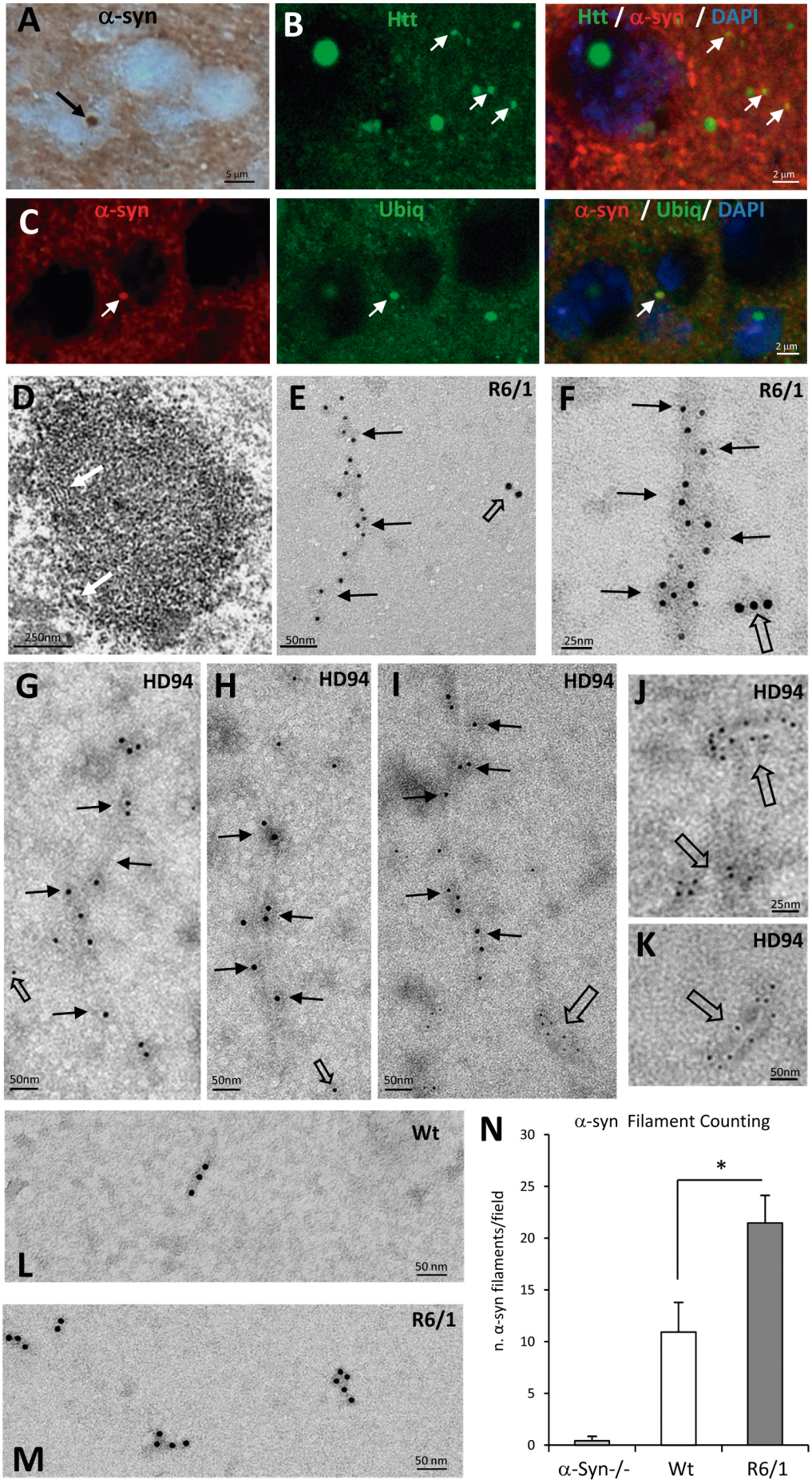
A
α-syn
5 µm
B
Htt
Htt / α-syn / DAPI
2 µm
C
α-syn
Ubiq
α-syn / Ubiq / DAPI
2 µm
D
250nm
E
R6/1
50nm
F
R6/1
25nm
G
HD94
50nm
H
HD94
50nm
I
HD94
50nm
J
HD94
25nm
K
HD94
50nm
Wt
L
50 nm
R6/1
M
50 nm
N
α-syn Filament Counting
n. α-syn filaments/field
30
25
20
15
10
5
0
*
α-Syn-/-
Wt
R6/1

Figure 2

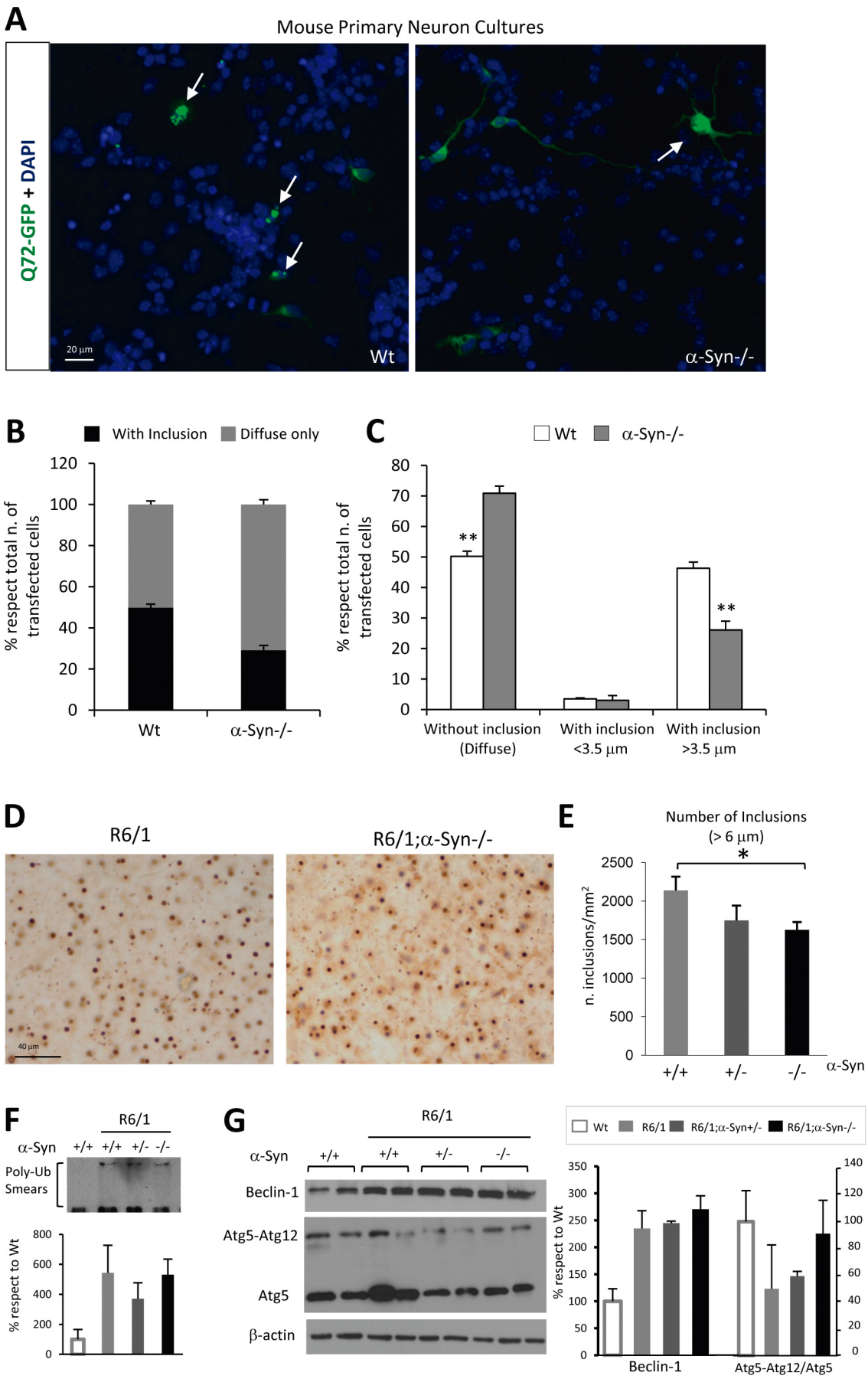
A
Mouse Primary Neuron Cultures
Q72-GFP + DAPI
20 µm
Wt
α-Syn-/-
B
With Inclusion
Diffuse only
% respect total n. of transfected cells
120
100
80
60
40
20
0
Wt
α-Syn-/-
C
Wt
α-Syn-/-
% respect total n. of transfected cells
80
70
60
50
40
30
20
10
0
**
**
Without inclusion (Diffuse)
With inclusion <3.5 µm
With inclusion >3.5 µm
D
R6/1
R6/1;α-Syn-/-
40 µm
E
Number of Inclusions (> 6 µm)
*
n. inclusions/mm²
2500
2000
1500
1000
500
0
+/+
+/-
-/-
α-Syn
F
R6/1
α-Syn
+/+ +/+ +/- -/-
Poly-Ub Smears
% respect to Wt
800
600
400
200
0
G
R6/1
α-Syn
+/+ +/+ +/- -/-
Beclin-1
Atg5-Atg12
Atg5
β-actin
Wt
R6/1
R6/1;α-Syn+/-
R6/1;α-Syn-/-
% respect to Wt
350
300
250
200
150
100
50
0
140
120
100
80
60
40
20
0
Beclin-1
Atg5-Atg12/Atg5

Figure 3

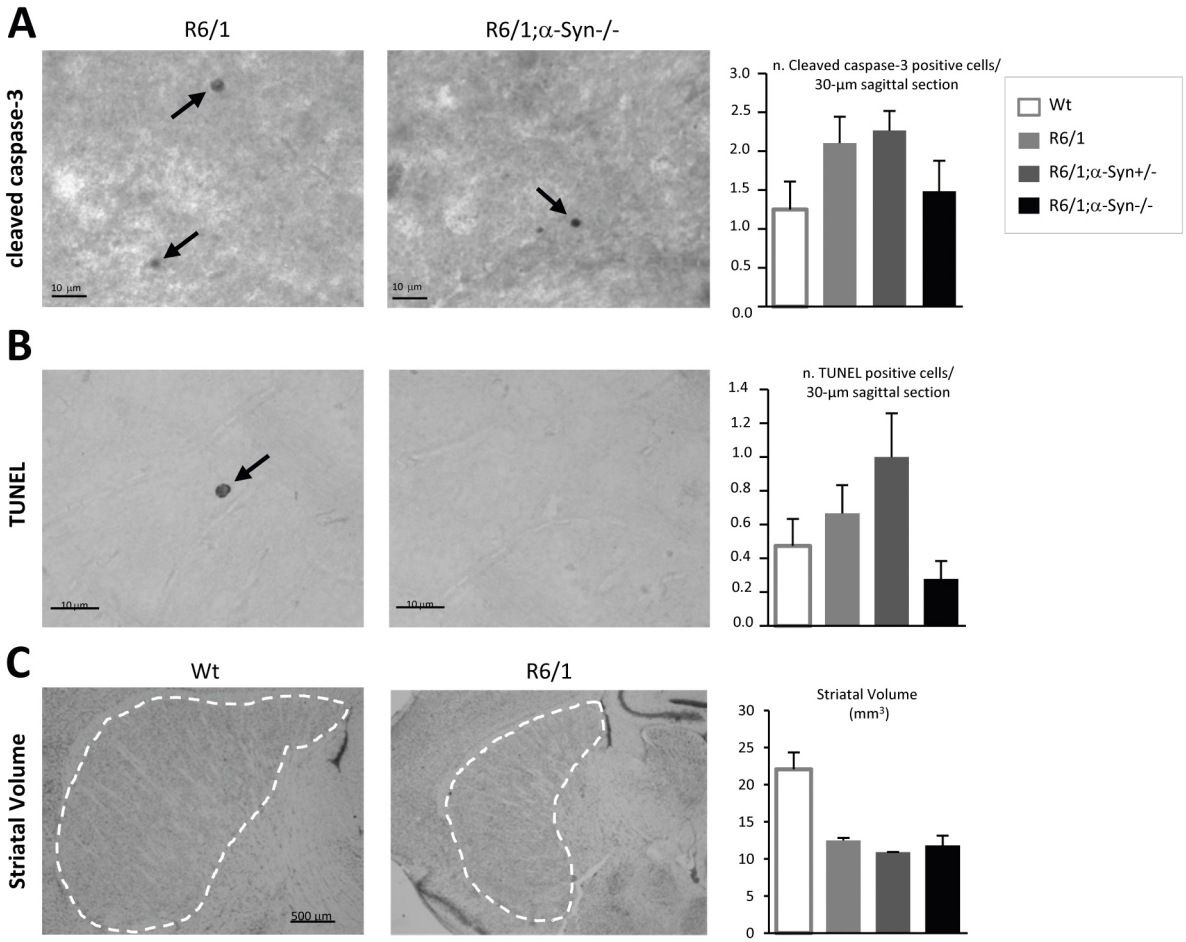
A
R6/1
R6/1;α-Syn-/-
cleaved caspase-3
10 μm
10 μm
n. Cleaved caspase-3 positive cells/
30-μm sagittal section
3.0
2.5
2.0
1.5
1.0
0.5
0.0
Wt
R6/1
R6/1;α-Syn+/-
R6/1;α-Syn-/-
B
TUNEL
10 μm
10 μm
n. TUNEL positive cells/
30-μm sagittal section
1.4
1.2
1.0
0.8
0.6
0.4
0.2
0.0
C
Wt
R6/1
Striatal Volume
500 μm
Striatal Volume
(mm3)
30
25
20
15
10
5
0

Figure 4

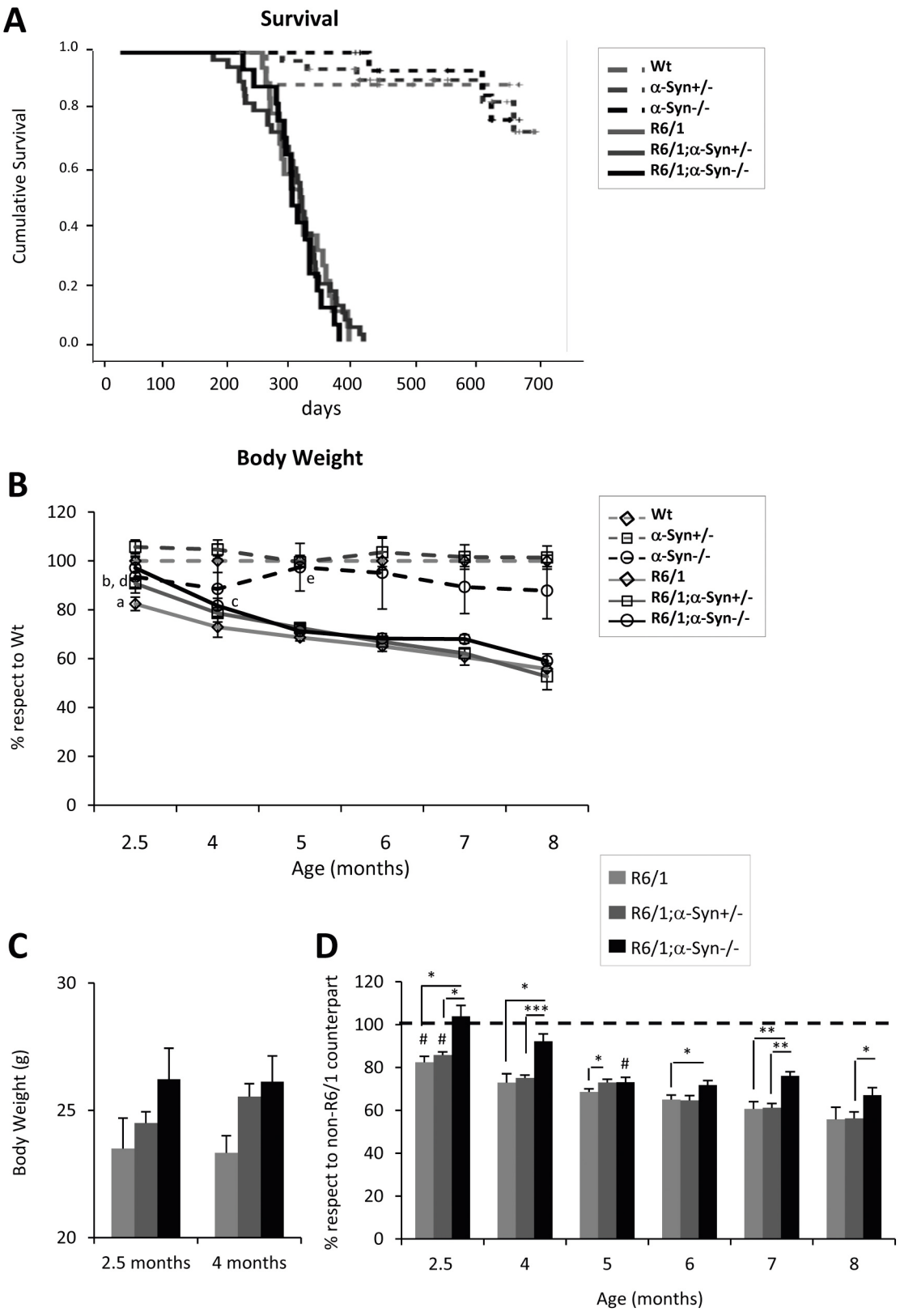
A
Survival
Cumulative Survival
1.0
0.8
0.6
0.4
0.2
0.0
0
100
200
300
400
500
600
700
days
Wt
α-Syn+/-
α-Syn-/-
R6/1
R6/1;α-Syn+/-
R6/1;α-Syn-/-
B
Body Weight
% respect to Wt
120
100
80
60
40
20
0
2.5
4
5
6
7
8
Age (months)
b, d
a
c
e
Wt
α-Syn+/-
α-Syn-/-
R6/1
R6/1;α-Syn+/-
R6/1;α-Syn-/-
C
Body Weight (g)
30
25
20
2.5 months
4 months
D
% respect to non-R6/1 counterpart
120
100
80
60
40
20
0
2.5
4
5
6
7
8
Age (months)
R6/1
R6/1;α-Syn+/-
R6/1;α-Syn-/-

Figure 5

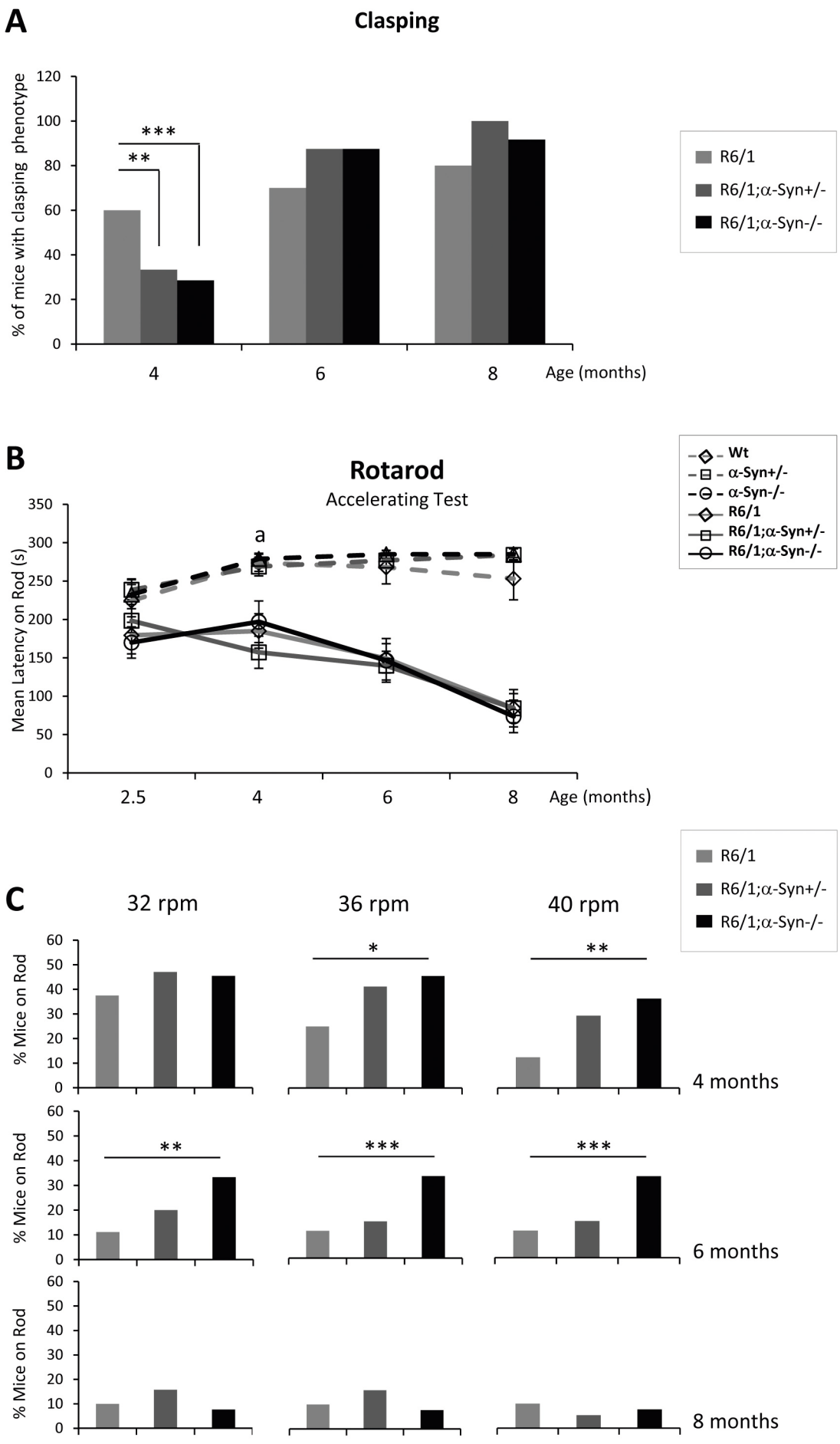
A
Clasping
% of mice with clasping phenotype
120
100
80
60
40
20
0
***
**
4
6
8
Age (months)
R6/1
R6/1;α-Syn+/-
R6/1;α-Syn-/-
B
Rotarod
Accelerating Test
Mean Latency on Rod (s)
350
300
250
200
150
100
50
0
a
2.5
4
6
8
Age (months)
Wt
α-Syn+/-
α-Syn-/-
R6/1
R6/1;α-Syn+/-
R6/1;α-Syn-/-
C
32 rpm
36 rpm
40 rpm
% Mice on Rod
60
50
40
30
20
10
0
*
**
**
***
***
4 months
6 months
8 months
R6/1
R6/1;α-Syn+/-
R6/1;α-Syn-/-

Figure 6

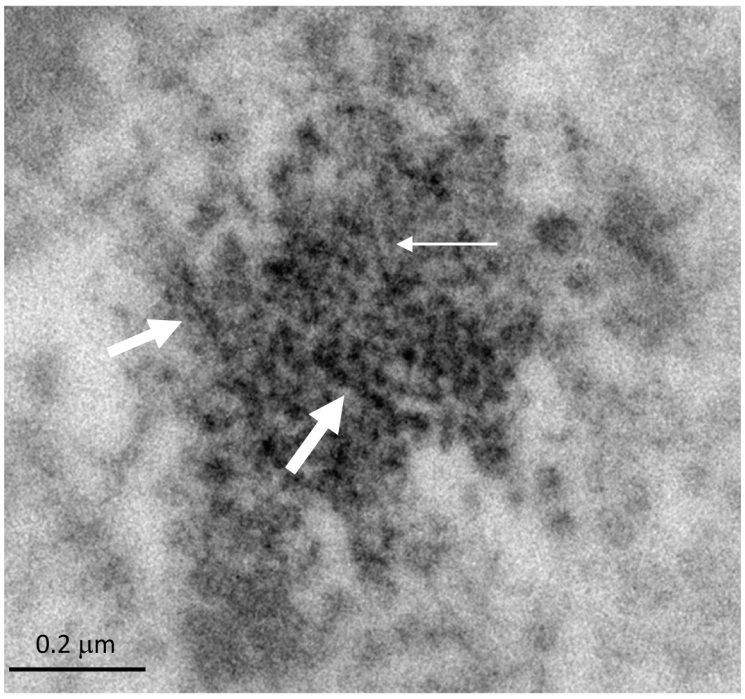

Supplementary Figure 1

A

Breeding Protocol

F_0 α-Syn-/- x R6/1

↓

F_1 α- Syn+/- x R6/1; α-Syn+/-

↓

B

Experimental Mice

F_2	Wt	α-Syn+/-	α-Syn-/-	R6/1	R6/1; α-Syn+/-	R6/1; α-Syn-/-
number	30	62	39	27	77	29

C

	Frequencies					
observed	11.4%	23.55	14.8%	10.2%	29.2%	11.0%
expected	12.5%	25%	12.5%	12.5%	25%	12.5%

Supplementary Figure 2